Heliyon 9 (2023) e17793

Contents lists available at ScienceDirect

Heliyon

journal homepage: www.cell.com/heliyon

Waste newspaper driven activated carbon to remove polycyclic aromatic hydrocarbon from wastewater

Aynun Nahar [a], Md. Ahedul Akbor [a,*], Nigar Sultana Pinky [b], Nushrat Jahan Chowdhury [a], Shamim Ahmed [a], Md. Abdul Gafur [c], Umme Sarmeen Akhtar [b], Md. Saiful Quddus [b], Fariha Chowdhury [d]

[a] Institute of National Analytical Research and Services (INARS), Bangladesh Council of Scientific and Industrial Research (BCSIR), Dhaka, Bangladesh
[b] Institute of Glass and Ceramic Research and Testing (IGCRT), Bangladesh Council of Scientific and Industrial Research (BCSIR), Dhaka, Bangladesh
[c] Pilot Plant and Process Development Center (PP&PDC), Bangladesh Council of Scientific and Industrial Research (BCSIR), Dhaka, Bangladesh
[d] Biomedical and Toxicological Research Institute (BTRI), Bangladesh Council of Scientific and Industrial Research (BCSIR), Dhaka, Bangladesh

ARTICLE INFO

Keywords:
Benzo[ghi]perylene (BghiP)
Indeno[1,2,3-cd]pyrene (IP)
Removal efficiency
Adsorption capacity
Adsorption isotherm
Adsorption kinetics

ABSTRACT

In this study, a carbon-based adsorbent was developed from waste newspaper through pyrolysis at 800 °C to evaluate the removal efficiency of polycyclic aromatic hydrocarbons (Benzo[ghi] perylene (BghiP) and Indeno [1,2,3-cd] pyrene (IP)) from wastewater. The surface area of the developed adsorbent was estimated at 509.247m^2g^{-1} which allowed the adsorption of the PAHs from wastewater. The maximum adsorption capacity was estimated at 138.436 μg g^{-1} and 228.705 μg g^{-1} for BghiP and IP, respectively and the highest removal efficiency was observed at pH 2. Around 91% removal efficiency was observed at pH 7 for both pollutants. Experimental adsorption data were fit for pseudo-second-order kinetics and Langmuir isotherm models, which demonstrate electrostatic interaction, monolayered deposition, hydrogen bonding, and π-π interaction between adsorbate and adsorbent which play a significant role in adsorption. The regeneration study described that the developed adsorbent could be able to intake 52.75% BghiP and 48.073% IP until the 8th and 6th cycles, respectively. The removal efficiency of the adsorbent in the real sample was also evaluated. This study will provide a method to convert waste material into adsorbent and will remove PAHs from wastewater as a function of pollutant mitigation and waste management.

1. Introduction

US Environmental Protection Agency (USEPA) and United Nations Environment Program (USEP) have categorized Polycyclic aromatic hydrocarbons (PAHs), which are defined priority pollutants due to their high toxicity [1,2]. As these chemicals are likely to have both natural and artificial origins associated with the incomplete combustion of organic materials [3] and the production of non-combusted [4] and petrogenic emissions [5], resultantly are widespread in the terrestrial [6], marine [7] and atmospheric

* Corresponding author. Principal Scientific Officer, Institute of National Analytical Research and Services (INARS), Bangladesh Council of Scientific and Industrial Research (BCSIR), Dhaka, 1205, Bangladesh.
E-mail addresses: aynunacce@gmail.com (A. Nahar), akbor@bcsir.gov.bd, akborbcsir@gmail.com (Md.A. Akbor).

https://doi.org/10.1016/j.heliyon.2023.e17793
Received 16 March 2023; Received in revised form 20 June 2023; Accepted 28 June 2023
Available online 29 June 2023

environments [8,9]. They enter into the ecosystem through natural processes such as volcanic eruption, forest burning, as well as through oil exploration and production processes, intentional burning of biomass [10] and fossil fuels [11], and incomplete combustion of other organic materials such as coal [5,12]. These pollutants accumulate in the food chain, resulting in unexpected effects and posing threats to humans and aquatic animals [13]. Since PAHs could pose negative consequences on the aquatic environment, it is pragmatic to develop an efficient treatment process for removing PAHs from wastewater [14]. Advanced oxidation, adsorption, membrane separation, photocatalysis, and biological degradation have been applied widely to investigate the removal efficiency of organic pollutants from wastewater [15,16,17,18]. Among several processes of treatment, adsorption is the most effective approach for removing organic pollutants derived from the ground, tap, and wastewater [19,20]. Noteworthy, a wide range of adsorbents e.g. biochar, activated carbon, and zeolite are typically employed to explore organic pollutants from wastewater [21]. Nowadays, biomass-producing waste (e.g. kapok fiber, biomass carbon, plant leaves, bamboo pulp fibers, etc.) based biochar has gained the attention of researchers considering waste management techniques aiming to apply an adsorbent for the removal of organic and inorganic pollutants from wastewater [22,23]. Likewise, waste newspaper-derived activated carbon (WNAC) can also be an alternative approach for treating PAHs contaminated water. A total of 49.4 tons of waste paper is produced in the capital of Bangladesh daily, and discharged into the environment [24]. Similarly, about 4 hundred million tons of waste paper is generated globally each year [25], in which vast portion of this belongs to newspapers. Hence, converting waste newspapers into carbon-based adsorbents for low-cost water remediation adsorbents has turned into the limelight of this current research. Pham et al. [6] suggested that waste paper aerogel has good adsorption affinity for phenol and chlorophenol, which also has had better antibiotics removal efficiency in wastewater [26]. Despite this, no study has been conducted so far to assess the PAHs adsorption onto WNAC.

A method for developing activated carbon from waste newspaper and its application will be established in this study, where the adsorbent employs the removal of Benzo [ghi] perylene (BghiP) and Indeno [1,2,3-cd] pyrene (IP) from wastewater. Moreover, batch studies were performed here to evaluate the effectiveness of WNAC. In addition, this study demonstrates a promising technique for utilizing waste material as an adsorbent that possesses a high surface area with adsorption capacity for organic pollutants in wastewater.

2. Materials and methods

2.1. Raw materials

The studied samples of waste newspaper (WN) were collected from the Institute of National Analytical Research and Services (INARS), Bangladesh Council of Scientific and Industrial Research (BCSIR), Bangladesh. In order to conduct laboratory studies, indeno [1,2,3-cd] pyrene (IP), and Benzo [ghi] perylene (BghiP) standards were delivered from Sigma-Aldrich (Kuri & Company, Dhaka, Bangladesh) along with HPLC-grade dichloromethane and ethanol. Mentioning, the remaining chemicals (e.g., $NaClO_2$, KOH, Na_2SO_4) were of analytical grade.

2.2. Sample preparation

Waste newspaper (WN) was collected and cut into 2 cm × 2 cm pieces. 1000 mL solution containing deionized (DI) water and ethanol (ratio 1:1) was added to 100 g of the WN in a 2000 mL glass beaker for 48 h. The prepared mixture was stirred mechanically for 48 h at a rotation speed of 2000 rpm to get a homogenous mixture pulp. Then the mixture was treated with the required amount of sodium chlorite in an acidic environment to remove ink and reduce the material's density, followed by stirring for another 30 h. Treated pulp was washed with DI water three times and then treated with 300 mL KOH solution for the next 60 h with continuous stirring at before mentioned rpm to produce homogeneous WN pulp (H-WNP). H-WNP was placed in a predetermined mold to get the convenient shape for the pyrolysis chamber board and then dried in an oven at 80 °C for 24 h. Required shaped dried samples were sent to the pyrolysis chamber. The pyrolysis was carried out at 800 °C under a nitrogen atmosphere with a heating rate of 5 °C min^{-1} for 3 h. After cooling to room temperature, the obtained products were soaked in 2 M HCl solution, followed by sonicated for 1 h, and then held overnight to remove encapsulated ash from the pores. Then the sample was washed with DI water and continued until the pH was neutral. Finally, the prepared activated carbon was dried for 48 h at room temperature and then stored in glass jars for further analysis.

2.3. Characterization

A scanning electron microscope (SEM) (Phenom Pro-Desktop 1481, USA) was applied to understand the surface morphology of the WNAC. The surface area, pore size, and pore volume of the WNAC were assessed also by using BET surface analyzer (BET-201-A, PMI, Tampa, FL, USA) using N_2 adsorbate with degassing temperature 120 °C (for 9 h) and the experiment was carried out at −195.76 °C. The chemical composition of the sample was determined by an Elemental Analyzer (Vario EL Cube, Elementar, Germany). The elemental composition of the WNAC surface was estimated to ensure PAHs adsorption utilizing X-ray Photoelectron Spectrometer (XPS) (Thermo Scientific K-Alpha X-ray Photoelectron Spectrometer, USA).

2.4. Adsorption experiment

To conduct batch experiments for determining adsorption capacity and removal efficiency, standard solutions of BghiP and IP were diluted to a predefined concentration ((50, 100, 150, 200, and 250 μg L^{-1} of BghiP) and (100, 200, 250, 300 and 400 μg L^{-1} of IP)) in

500 mL volumetric flask with distilled water. The effect of initial concentration, adsorbent dosages, and pH of the initial solution was determined through batch experiments with three repetitions. To assess the impact of the dosage, different dosages (0.02, 0.04, 0.05, 0.06, 0.08, and 0.1 g) of WNAC were added into a 50 mL solution of BghiP with a concentration of 150 μg L^{-1}. For IP, different dosages (0.02, 0.04, 0.05, 0.06, 0.08, and 0.1 g) of WNAC were put into 50 mL 250 μg L^{-1} IP solution. Where 150 μg L^{-1} for BghiP and 250 μg L^{-1} for IP optimum concentration were considered for further batch experiments. Each prepared mixture was placed in an orbital shaker at 200 rpm for 6 h at room temperature to obtain an adsorption equilibrium. A blank standard containing only PAHs without adsorbent was performed for each concentration. The organic portion was separated, filtered (through a 0.45-μm membrane filter), and sent for further analysis with a gas chromatograph-mass spectrometer (GC-MS). In addition to determining the initial pH effect, the optimum concentration with different pH solutions (2, 4, 7, 10, and 12) for each PAH with an optimum dose and volume was added to obtain equilibrium. A batch experiment had been done using the optimum concentration of BhiP with a volume of 50 mL with an optimum dose of 0.05 g for 6 h at 200 rpm rotation. Like BghiP, a batch experiment with an optimum concentration of 250 μg L^{-1} for IP having a volume of 50 mL with an optimum dose of 0.05 g for 6 h at 200 rpm rotation. NaOH (0.1 mol L^{-1}) and HCl (0.1 mol L^{-1}) were used to adjust the initial pH to 2, 4, 7, 10, and 12. After attaining equilibrium, the organic portion of each sample mixture was separated, filtered, and sent for GC-MS analysis. The effect of contact time was evaluated too.

The equations were applied to calculate the amount of PAHs adsorption onto the adsorbent and the removal efficiency.

$$qe = (Co - Ce)V / m \tag{1}$$

$$Re = (Co - Ce) \times 100 / Co \tag{2}$$

Where, the adsorption capacity of BghiP or IP on WNAC (μg g^{-1}) denotes qe, Re (%) is the removal efficiency of BghiP or IP through the adsorbent, and Co and Ce are represented as initial time and equilibrium time (μgL^{-1}) concentrations of BghiP or IP respectively. The volume of the adsorbate solution is represented as (L), and m is the weight of the adsorbent (g) [13,13].

2.5. Equilibrium isotherm models

As explained earlier, different concentrations for each PAH with an optimum dose (0.05g) and volume (50 mL) were applied to conduct a sorption isotherm at room temperature as per Langmuir and Freundlich models with three replications (Supplementary file, S1). Likewise, the same experimental conditions were used to perform the equilibrium isotherm experiment. Ref. [27,28] demonstrates that the PAH removal efficiency is higher at room temperature compared to other increasing temperatures since adsorption is inversely proportional to the temperature. Thus, the selection of room temperature for isotherm studies was implemented in this study to delineate optimum removal efficiency.

2.6. Adsorption kinetics

The optimum concentration with an optimum dose for each PAH was applied to evaluate the adsorption kinetics namely pseudo-first-order (PFO) and pseudo-second-order (PSO) models consecutively (Supplementary file, S2). Samples were collected at 30, 60, 120, 180, 300, and 360 min with three replicates followed by the aforementioned conditions.

2.7. Regeneration study of WNAC

Adsorption of each PAH onto WNAC was carried out by applying optimum conditions. After equilibrium, a desorption study was performed using 40% ethanol solution at room temperature to desorb adsorbate from the adsorbent. Finally, the adsorbent was washed with DI water, dried for 6 h at 80 °C, and then sent for further reabsorption studies.

2.8. GC-MS analysis of PAHs

The way of sample preparation technique was followed as documented by Qiao et al. [29] with few modifications. Firstly, the organic phase was extracted through 20 mL dichloromethane (DCM) from the solution. A required quantity of anhydrous sodium sulfate was added to remove moisture from extracted portion aiming to turn the volume at 10 mL solution via a rotary vacuum evaporator. Secondly, the resultant volume was moved through the alumina and silica gel column with a ratio of 1:2 to remove impurities. Eventually, the obtained elute was concentrated again with the rotary vacuum evaporator to 2 mL, which, in turn, was stored in 2 mL glass vials for further analysis by Shimadzu gas chromatograph coupled to the mass spectrometer (GC-MS) (Simadzu 2010 plus, Japan) to get SH-Rxi 5sil capillary column (30.0 m × 0.25 mm × 0.25 μm) along with following operating conditions: 60–280 °C oven temperature, 1.0 μL injection volume with a split-less injection mode, 1.00 μL min^{-1} column flow, 250 °C detector temperature, and N_2 as carrier gas.

3. Results and discussion

3.1. Characterization of WNAC

3.1.1. Surface area

According to BET analysis, WNAC illustrated that type I adsorption-desorption isotherms with a hysteresis loop H4, representing a microporous structure on the surface (Fig. 1a). In Fig. 1b, the pore size ranges between 0.01 and 10 nm, implying the availability of both micro and mesopores on WNAC surface. The specific surface area and pore volume of WNAC were detected at 509.247 $m^2\ g^{-1}$ and 0.3634 $cm^3\ g^{-1}$; whereas micropore and mesopore surface areas were 390.246 $m^2\ g^{-1}$ and 119.001 $m^2\ g^{-1}$, respectively. The availability of micropores compared to mesopores in the WNAC indicates that KOH treatment leads to a higher surface area. It happens because KOH treatment may decompose the volatile compounds which leads to the generation of higher micropore in surface area [30]. The finding of this study is similar to the other studies ref. [13,31].

3.1.2. Surface morphology and internal structure

The surface morphology and internal porosity greatly influence the adsorption of PAHs onto the adsorbent [28,32]. The orientation of fibers in the WNAC is almost irregular, and maintained a twisted network (Fig. 2). This irregular twisted network results in a non-uniform distribution of pores on the surface of WNAC. As mentioned, the high porosity of WNAC provides a more active site for contaminant adsorption [33,34], which is very consistent with those studied by Refs. [26,35].

3.1.3. Surface chemistry

According to XPS profiling, the WNAC contains C and O possessing the characteristic peaks at 284.6 eV and 532.2 eV (Fig. 3a). Besides three distinct peaks for C1s were detected at 284.76, 285.86, and 288.47 eV with high resolution. Where the peak at 284.76 eV represents the availability of aliphatic carbon. The next peak at 285.86 eV implies that C is singly bonded to oxygen, while the peak at 288.47 eV indicates that C is singly bonded to oxygen [36,37]. In Fig. 3b, C1s showed three characteristic peaks at 284.76, 285.86, and 288.47eV, indicating the presence of C and O. Moreover, a satellite peak was detected at 291.3 eV, indicating the presence of the aromatic compound in WNAC that confirmed the adsorption of BghiP and IP onto the WNAC.

3.1.4. Chemical composition

H-WNP is constituted of 41.93% C, 6.747% H, and 0.19% N, whereas WNAC contains 82.01% C, 1.260% H, and 0.44% N. A higher percentage of carbon in WNAC indicates a higher degree of carbonization and purity of the WNAC [30,38].

3.2. Adsorption study of WNAC

3.2.1. Effect of dosage forms

The dosage form plays a crucial role in the adsorption capacity of WNAC. The removal efficiency of the adsorbent is sharply raised from 65.074% to 94.741% with the dosage between 0.02 and 0.05 g (Fig. 4a). The availability of active sites for the adsorption of pollutants might be the possible reason for this sharp increase [39]. Although a gradual increase in removal efficiency to 94.958% is observed with a further rise of dosages from 0.06 to 0.10 g. Overcrowding of adsorbate molecules results from overlapping of adsorbent sites at high adsorbent dose which causes unsaturation in the increased active sites and facilities gradual rise despite faster at high adsorbent dosage [40,41]. Similarly, for IP, a significant Re is observed for dosage from 0.02 to 0.06 g with a value between

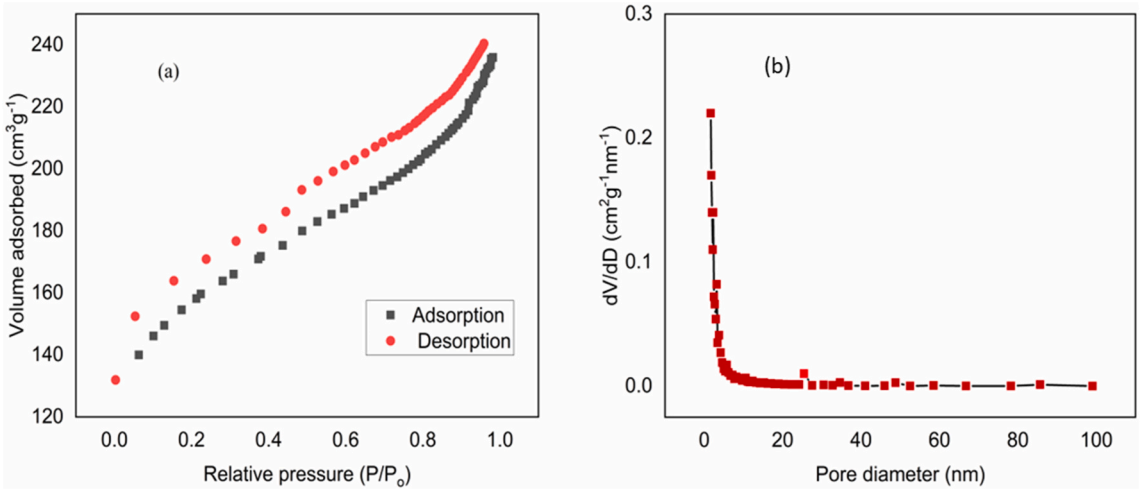

Fig. 1. (a)Adsorption-desorption isotherm and (b) BJH pore size distribution of WNAC.

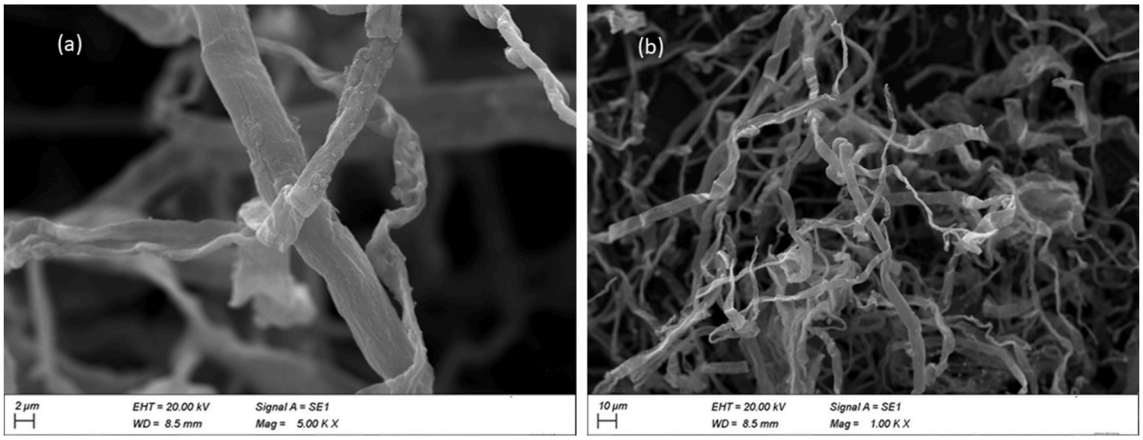

Fig. 2. Surface morphology of WNAC: (a) fibre like structure and (b) irregular twisted network.

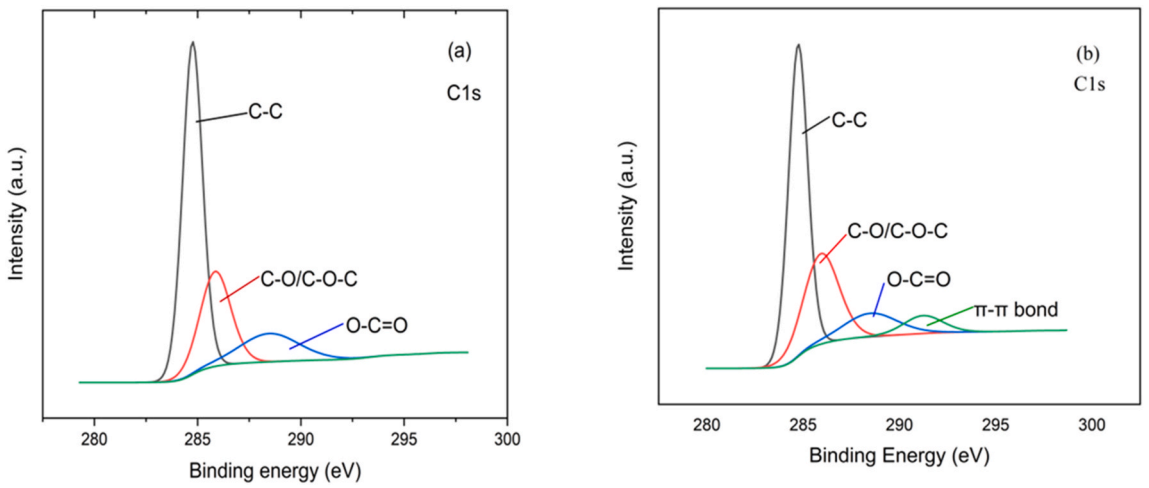

Fig. 3. Surface chemistry: (a) C1s XPS profile of WNAC, and (b) C1s XPS profile of PAHs adsorbed WNAC.

57.644% and 92.374% (Fig. 4a). However, a slight decline in removal efficiency is observed to 0.1 g. Unsaturation of adsorbent sites due to overcrowding of adsorbate molecules might be the probable reason for this decline [40,41]. Li et al. [22] reported that the removal efficiency of *p*-nitrophenol through activated carbon aerogels (ACA) was increased quickly to 96.2% up to dosage 0.4 g L^{-1}, and then the increase of rate gradually slows down at higher dosage. Qiao et al. [24] stated that PYR and BaP removal efficiencies rose sharply with the increase of EP-biochar dosage up to 0.05g compare to higher dosages (>0.05 g).

3.2.2. Effect of initial concentration

In Fig. 4b, the removal efficiency of NWAC declines with increasing the initial concentration. BghiP adsorption capacity of adsorbent is estimated high at lower concentrations (50–150 µg L^{-1}) compared to the higher concentrations (200–250 µg L^{-1}). At low concentrations, available active sites for adsorption onto adsorbent are present for the uptake of adsorbate molecules, which results in a higher rate of removal efficiency. In contrast, a decline in removal efficiency with the increased initial concentration could be related to the saturation of active sites of adsorbent after equilibrium [24]. Since the number of active sites for the given amount of adsorbent dose remains the same compared to the increased number of BghiP molecules leading to declining the adsorption capacity at higher concentrations. This phenomenon is occurred because of the saturation of adsorption sites by a fixed amount of adsorbent at the equilibrium point of adsorption [29,31,42]. Based on the removal efficiency, it can be inferred that NWAC can effectively be removed from the lower concentration adsorbate (≤150 µg L^{-1}) in solution.

The removal efficiency of IP declined with an increase in its initial concentration (Fig. 4b). This is because of the higher degree of saturation of adsorbent at higher concentrations [33]. Up to 250 µg L^{-1}, more than 90% removal efficiency is observed, but the removal efficiency dropped significantly at 300 µg L^{-1} and continued to decline with increasing IP content in the experiment solution, which resembles the findings of [13,22]. Ref. [24] cited that PYR and BaP removal efficiencies were decreased with the increase of higher initial concentration due to saturation of adsorbent after equilibrium.

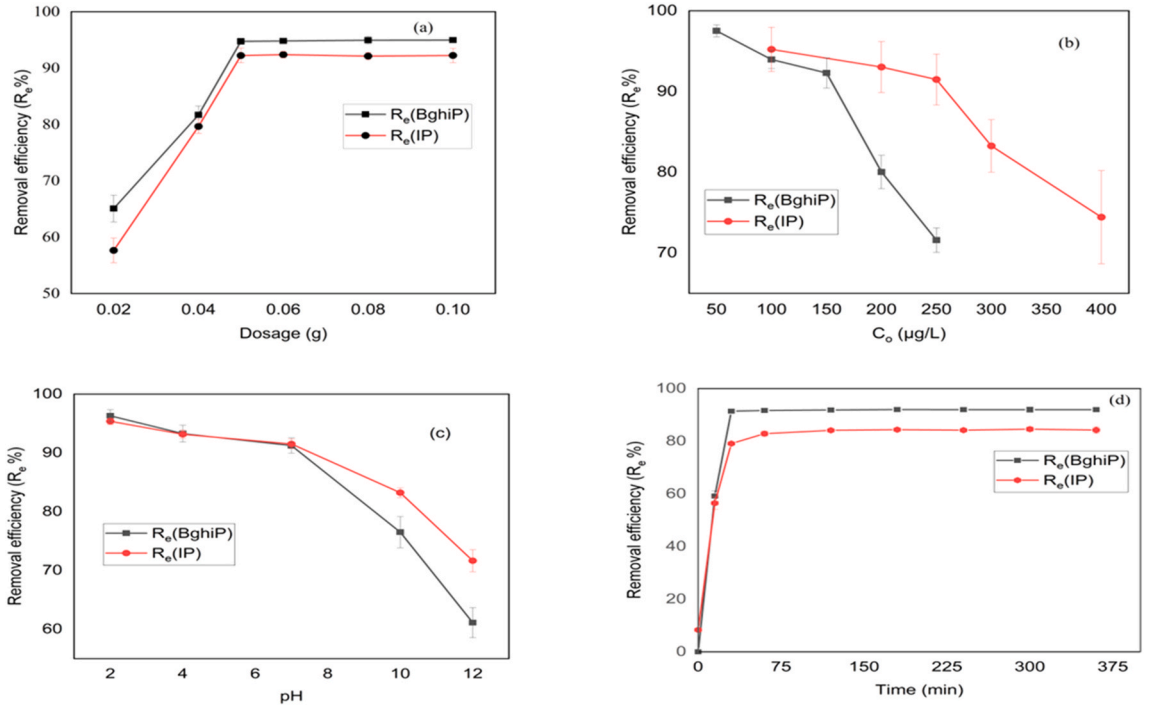

Fig. 4. Effect of parameters in adsorption: (a) dosage (b) initial concentration (c) pH and (d) time.

3.2.3. *Effect of solution pH*

Investigation of the effect of pH on PAHs adsorption has been carried out at five distinct pH of 2, 4, 7, 10, and 12. The PAHs removal efficiency through NWAC is decreased with an increase in pH, and optimum removal efficiency is found at the lowest pH. This is because at pH below 7, PAH molecules become protonated and act as electron acceptors (Lewis acid). Besides, surface carboxyl groups on NWAC act as electron donors (Lewis base). Thus, they form an electron-donor–acceptor (EDA) complex and promote the adsorption process at lower pH [13,27,43]. Reversely, at higher pH (>7), PAHs molecules associate as negatively charged ions and active sites of NWAC became negatively charged which results in electrostatic repulsion between PAHs and adsorbent, impose slowing down the removal efficiency [13,27]. Fig. 4c shows 96.303% BghiP removal efficiency at pH 2; while 61.122% removal efficiency at pH 12 onto NWAC. IP also showed a similar function as occurred for BghiP, where the highest percentage of removal efficiency (95.373%) is observed at the lowest pH. Conversely, the lowest removal efficiency (71.655%) is estimated at the highest pH (Fig. 4c). Noteworthy, ref. [13,22,36] cited that the removal efficiency of benzene ring-containing organic pollutants is dropped at higher pH. Ref. [8] stated that benzene rings containing Ph and 2CP show better interaction toward carbon aerogel at lower pH; since glucose-driven carbon aerogel showed 97% nitrophenol removal efficiency in the acidic environment [22]. Oh et al. [36] investigated that the sorption of 2, 4-dichlorophenol (DCP) onto polypropylene/rice straw (PP/RS) derived biochar at pH 4.7 was slightly higher than that at 7.4.

3.2.4. *Effect of contact time*

To estimate the required equilibrium time, the removal efficiency of BghiP onto WNAC is studied as a function of the contact time. Fig. 4d shows that adsorption is found higher at the onset of the experiment due to the availability of a higher number of active adsorption sites for the removal of BghiP. Around 92% removal is observed over nearly 30 min duration followed by a slow equilibrium approach. This is because the lower energy surface sites are initially saturated with adsorbate molecules, resulting in faster adsorption at the beginning [6]. In turn, the adsorbate molecules are transferred into higher energy surface sites which leads to a lower removal rate due to surface and pore blockage of the adsorbent surface [35]. At the equilibrium stage, adsorbate molecules are occupied by the maximum active sites which makes it difficult to adsorb high adsorbate [44,45].

Compared to BghiP, the adsorption rate is recorded high at the initial condition and showed about 92% removal over 60 min duration, which eventually turns to equilibrium slowly (Fig. 4d), because blockage of the available active site is noticed for the adsorption [13,44,45]. Similar findings are observed from the studies; adsorption of organic solvents (phenol and 2- chlorophenol (2CP)) [13] and antibiotics (vancomycin) [26] onto waste paper-derived carbon aerogel. Ref. [13] stated that approximately 80% removal efficiency was found within 10 min; whereas ref. [21] reported that 90% removal efficiency was attained in 40 min.

3.3. *Study of adsorption isotherm*

The adsorption isotherms are performed to determine whether the model is best fitted to the adsorption of PAHs. As given all

parameters in Table 1 and Fig. 5a –b, the BghiP adsorption onto NWAC followed the Langmuir model with a higher correlation coefficient value ($R^2 = 0.963$) rather than the Freundlich model ($R^2 = 0.900$), indicating monolayer and homogeneous adsorption of BghiP on the adsorbent surface [35,40,46]. At room temperature, the maximum adsorption capacity (q_{max}) of BghiP is assessed at 185.198 μg g^{-1} by applying the Langmuir model. In contrast, in the Freundlich model (Table 1), the calculated value of nf is greater than 1, representing the favorability of BghiP adsorption onto WNAC [47,48].

All parameters in Table 1 and Fig. 5c –d suggest that the Langmuir model fits better ($R^2 = 0.971$) than the Freundlich model ($R^2 = 0.865$) for IP adsorption onto NWAC. R^2 (Langmuir)> R^2 (Freundlich) demonstrates that adsorption occurred on the homogeneous surface of the adsorbent through monolayer deposition of adsorbate molecules and favors the Langmuir model. At room temperature, the maximum adsorption capacity of IP is assessed 320.223 μg g-1 through the Langmuir model. Like BghiP, the inclination of IP adsorption onto adsorbent is confirmed by nf value (>1), indicating the favorability of IP adsorption [41,42]. K_f is estimated at 82.480 μg g-1 $(L\mu g^{-1})^{1/n}$. Hence, the higher correlation coefficient value of the Langmuir model confirmed that BghiP and IP adsorption occurred through monolayer deposition on the homogeneous surface of NWAC. Ref. [13] concluded that the adsorption of Ph and 2CP on CA followed the Langmuir model with a maximum adsorption capacity of 238 and 278 mgL^{-1}, respectively. A similar observation was concluded by Qiao et al. [24], where PAHs sorption on biochar happened through monolayer and homogeneous adsorption.

3.4. Study of adsorption kinetics

Adsorption kinetics is frequently applied to understand adsorbate uptake by the adsorbent, which determines the contact time of adsorbate intake at the solid-liquid interface via numerous processes, such as diffusion, hydrophilic contact, chemisorption, etc. Fig. 6a-b and Table 2 represent the plot of kinetic models (PFO and PSO) and kinetic parameters for BghiP adsorption onto WNAC using experimental data, where, the pseudo-first-order model (PFO) model attributes less fitting with an R^2 value of 0.977; however, the pseudo-second-order model (PSO) exhibits best fitting with an R^2 value of 0.982 which implies that the adsorption process follows the pseudo-second-order kinetic model. This finding is consistent with the studies of [29], and [49]. Hence, it is assumed that the PSO model might be the rate-controlling stage in the adsorption of BghiP onto WNAC [26,49,50]. Fig. 6c-d and Table 2 demonstrate that the PSO model fits better as the rate-determining stage rather than PFO for IP, like BghiP. As given in Table 2, the R^2 value was assessed greater for PSO than PFO, confirming a favorable condition for the PSO adsorption kinetics model and also, the adsorption of adsorbate onto adsorbent is carried through the chemisorption process [26].

3.5. Adsorption mechanism

Adsorption of pollutants from an aqueous solution onto an adsorbent depends on the nature of the adsorbate [51], the chemical composition of the adsorbent, environmental conditions, etc. [52]. The SEM and BET studies confirmed the large surface area, high porosity, and a large number of available active sites of WNAC that results in the pore filling, entrapment, and diffusion of PAH molecules onto the adsorbent.

In addition, the presence of C═O, O–C–O, and O–C═O groups on the surface of the adsorbent (confirmed by XPS) acts as donors, and aromatic rings act as a receiver and promote the adsorption process by forming electron-donor–acceptor (EDA) complex [53]. The hydrogen of PAH forms hydrogen bonds with existing oxygen groups on the adsorbent surface and played a significant role in PAHs adsorption [6]. Additionally, adsorbent and adsorbate are carrying a high number of aromatic π electrons, leading to π-π bond formation between WNAC and PAHs [24,25,54,47,48,49]. XPS profiling of 1Cs, a satellite peak at 291.3 eV, also confirms that π-π interaction plays a major role in PAHs absorption onto adsorbent [50]. Therefore, adsorption of BghiP and IP have followed both physisorption (pore filling, entrapment, diffusion, etc.) and chemisorption (π-π interaction, EDA complex, etc.) mechanisms for adsorption of BghiP and IP onto NWAC. Similar findings were observed for PAHs adsorption for biochar from different raw materials in Refs. [13,49], and [55]. Pham et al. [13] stated that the adsorption of Ph and 2CP onto carbon aerogel followed the physisorption and chemisorption mechanism. Zhou et al. [44] reported that the adsorption mechanism of PAHs had occurred through π-π interaction between adsorbent and adsorbate along with a hydrophobic effect. Ref. [48] concluded that the electron cloud of PHE overlapped with the lone pair electron of N-doped biochar and π electron of aromatic rings which results in stronger binding ability; hence, facilities adsorption ability.

Table 1
Adsorption parameters of the Langmuir and Freundlich isotherms for BghiP and IP.

Model	Parameters	BghiP	IP
Langmuir adsorption isotherm	q_{max}(μg g^{-1})	185.198	320.223
	K_L(L μg^{-1})	0.215	0.097
	R^2	0.963	0.971
Freundlich adsorption isotherm	n_f	3.799	3.509
	K_f ((μg g^{-1})(L$\mu g^{-1})^{1/n}$)	60.618	82.480
	R^2	0.900	0.865

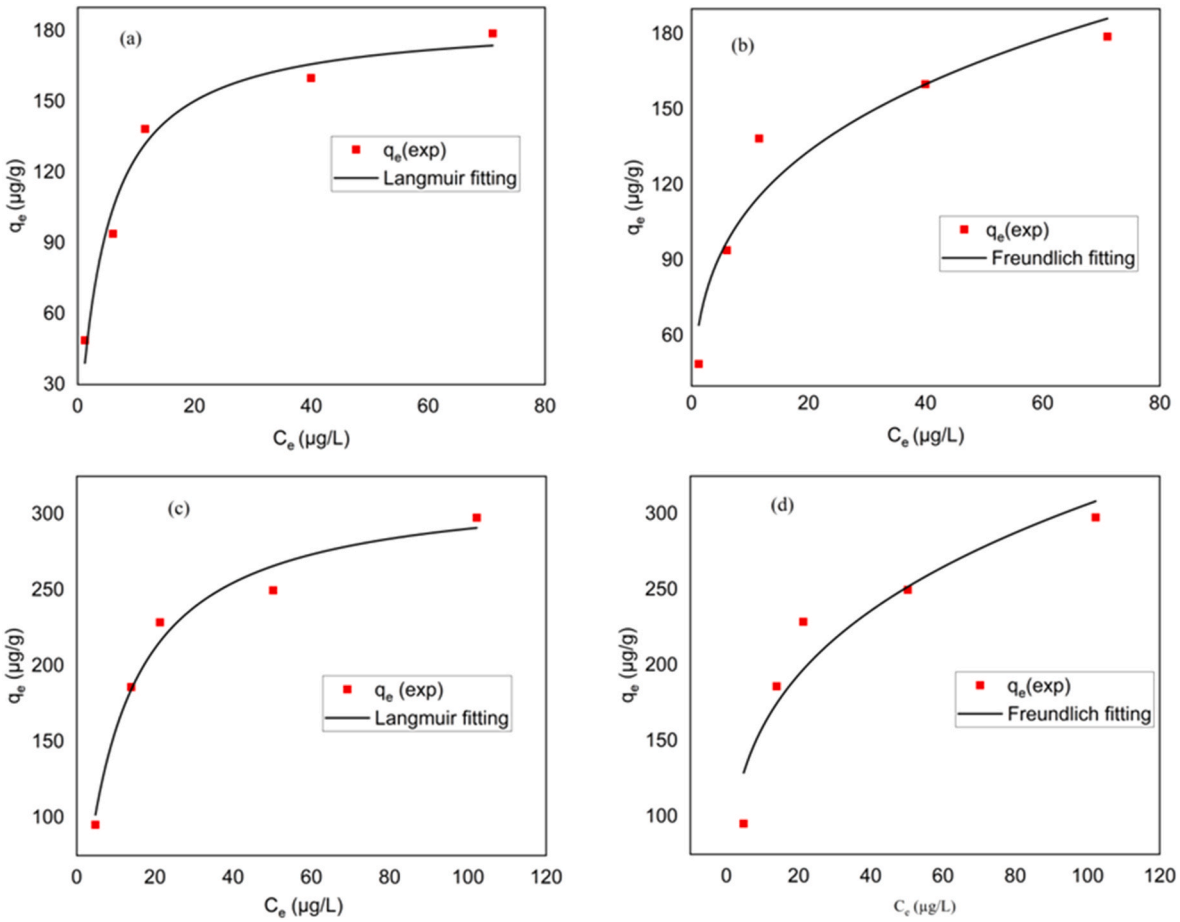

Fig. 5. Adsorption isotherms: Langmuir model (a) and Freundlich model (b) for BghiP; Langmuir model (c) and Freundlich model (d) for IP.

3.6. Regeneration study of WNAC

The regeneration study of adsorbent was done to estimate its efficiency for practical application [56]. The reusability experiment of adsorbent was done until eight cycles through simultaneous adsorption and desorption cycles. For the initial three cycles, the removal efficiency of the adsorbent was almost the same (around 90%) (Fig. 7a), then decreased gradually in the next five cycles, and removal was estimated at 52.75% in the last cycle. The blocking of pores by BghiP and irreversible adsorptive sites on the adsorbent surface might be the possible reasons for the decline in removal efficiency [6].

For IP, the regeneration experiment of adsorbent was done until the sixth cycle through simultaneous adsorption and desorption cycles. In the regeneration study, IP shows less removal efficiency compared to BghiP. As shown in Fig. 7 (b), the removal efficiency decreased drastically after the third cycle from 81.529% to 48.073%. Irreversible adsorptive sites of adsorbent together with pores blocking might be the probable reasons for this discrepancy [6].

3.7. Application using real sample

Water sample (pH: 7.07; dissolved oxygen: 4.65, electrical conductivity: 166.9 µscm^{-1}; TDS: 81.5 mgL^{-1}) was collected from the Turag River (23.857731 N, 90.344942E), Dhaka, Bangladesh, and the concentration of BghiP and IP was detected below the detection limit. To evaluate the removal efficiency of the adsorbent in a real sample, the optimum concentration of each PAH was added to the river water, and the experiment was conducted by applying optimum conditions. A slight decline in removal efficiency was observed for both pollutants compared to the lab experiment. The calculated removal efficiency was 87.041% and 85.632% for BghiP and IP respectively. This observation confirmed that WNAC would be a potential adsorbent for BghiP and IP remediation in the surface wastewater sample, although removal efficiency was lower in the real sample compared to the experimental sample. Matric interference might be the probable reason for this decline. Ref. [13] showed that the removal efficiency of carbon-based aerogels derived from waste paper (CWP) was declined for synthetic wastewater samples containing targeted contaminants (Ph, 2CP, NO_3^-, SO_4^{2-}, PO_4^{3-}, Cu^{2+}, Mg^{2+}, Ca^{2+}, Pb $^{2+}$, Cd $^{2+}$) rather than single contaminant system in lab experiment. This may come from the interference effect of the coexisting metal ions or other anions in the synthetic wastewater sample and the completion of adsorption of the Ph and 2CP

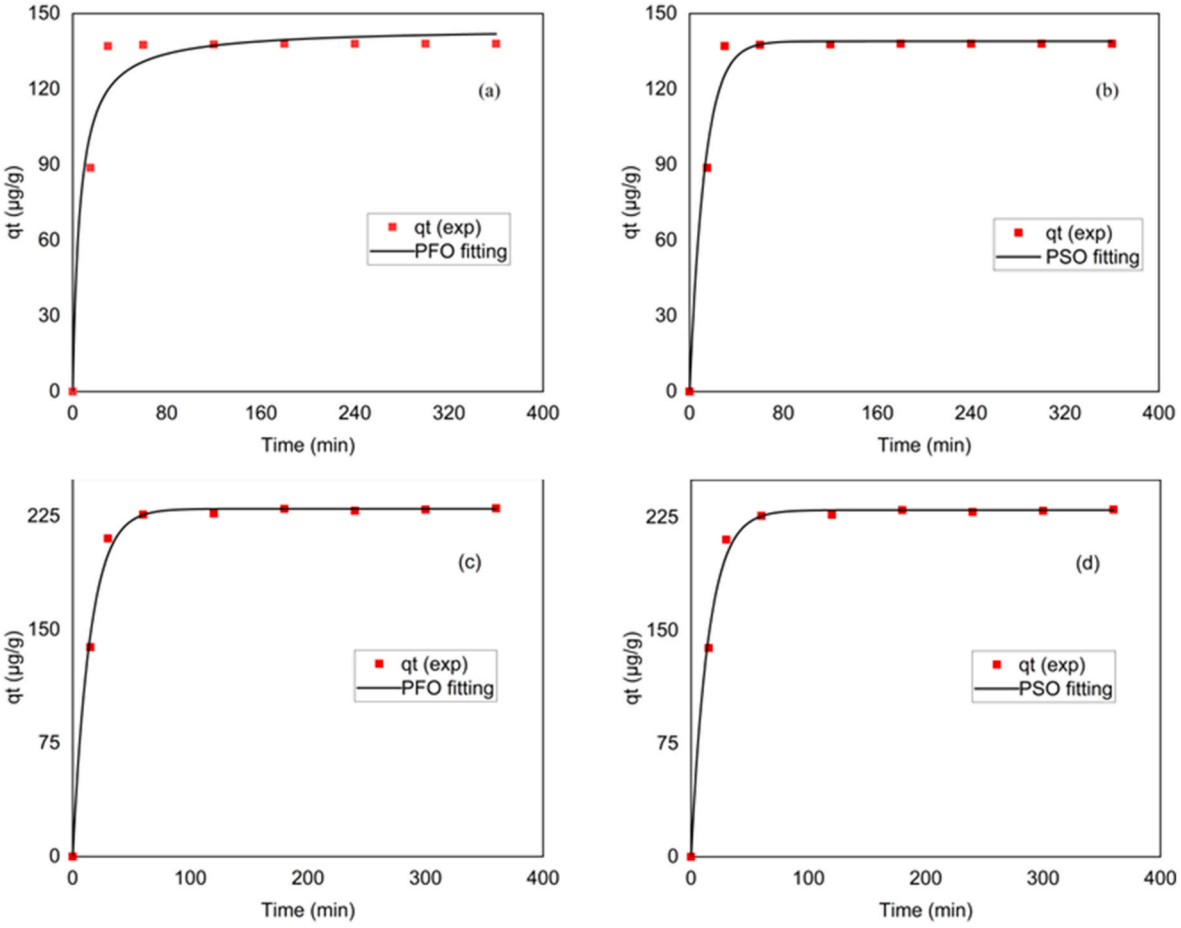

Fig. 6. Adsorption kinetics: PFO (a) and PSO (b) for BghiP; PFO (c) and PSO (d) for IcdP.

Table 2
Adsorption parameters of the pseudo-first and second order kinetics for BghiP and IP.

Reaction order	Parameters	BghiP	IP
Pseudo-first-order model	q_e (μg g^{-1})	139.026	228.726
	K_1 (min^{-1})	0.078	0.072
	R^2	0.977	0.9963
Pseudo-second-order model	q_e (μg g^{-1})	144.341	232.279
	k_2 (g μg^{-1} min^{-1})	0.00112	0.00138
	R^2	0.982	0.9993
Experimental adsorption capacity at equilibrium	$qe_{exp.}$ (μg g^{-1})	138.436	228.705

molecules onto the surface of CWP. Ref. [50] reported higher removal efficiency of BaA, BbF, BkF, and BaP for real samples (seawater and river water) application compare to lab study by using coconut waste and orange waste biochar, although lower removal efficiency was achieved for DahA. This is because the greater ionic effect of the matrices might facilitate the removal efficiency of the PAHs from real samples.

3.8. Comparison with other studies

Several adsorbents were used for removing PAHs from an aqueous solution (Table 3). Ref. [29] reported that *Enteromorpha prolifera* (EP) biochar had shown a maximum adsorption capacity of 187.27 μg g^{-1} and 80.00 μg g^{-1} for the pollutants named Pyrene (PY) and benzo[a]pyrene (BaP), respectively. They also reported that adsorption behavior suits the Langmuir model and SO reaction model, which is consistent with this study. Gupta et al. (2016) [41] investigated banana peel biochar's adsorption capacity for Anthracene. Another investigation was done by de Jesus et al. [43] estimating the adsorption capacity of coconut waste biochar for five PAHs (BaA, BbF, BkF, BaP, and DahA) where BaA showed a maximum adsorption capacity of 19.09 μg g^{-1} with a removal efficiency of 86.09%.

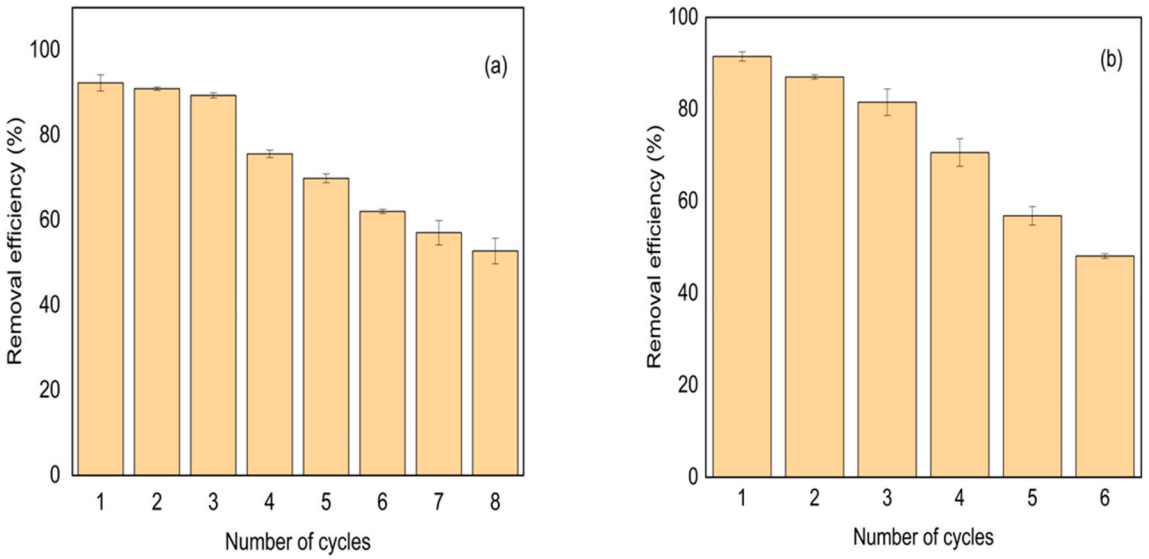

Fig. 7. Regeneration study: (a) BghiP and (b) IP.

Table 3
Comparison with other studies.

Sl. No.	Adsorbent	Adsorbate	Adsorption capacity	Surface area (m^2 g^{-1})	Ref.
1.	Enteromorpha prolifera biochar	PY and BaP	187.27 and 80.00 μg g^{-1}	205.32	[29]
2.	Banana peel biochar	A	357.14 μg g^{-1}	–	[41]
3.	Coconut waste biochar	BaA, BbF, BkF, BaP and DahA	19.09, 17.44, 15.79, 12.56, and 8.31 μg g^{-1}	233.87	[50]
4.	Wood waste-derived biochar	BghiP and IP	0 and 1 μg g^{-1}	864	[49]
5.	Laccase-carrying electrospun fibrous membrane	PHE, BaA, and BaP	2239, 1339, and 872 μg g^{-1}	229.25	[57]
6.	Graphene Oxide aerogel	BaP	0.310 μg g^{-1}	200	[58]
7.	Petroleum coke-based activated carbon	PHE	46 μg g^{-1}	562	[59]
8.	WNAC	BghiP and IP	138.436 and 228.705 μg g^{-1}	509.247	This study

Zhou et al. [49] investigated the adsorption capacity of wood waste-derived biochar for 16 PAHs and demonstrated that PAH adsorption energy was mostly affected by the number of rings in benzene. Also, the adsorption capacity of BghiP and IP by biochar were detected 0 μg g^{-1} and 1 μg g^{-1} respectively which is much lower than the experimental values of this study. Biochar showed very negligible removal efficiency compared to NWAC, although surface area of biochar (864 m^2 g^{-1}) was reported higher than NWAC (509.247 m^2 g^{-1}). Ref. [57] demonstrated that laccase-carrying electro spun fibrous membrane had shown outstanding adsorption capacity for phenanthrene (PHE), benzo(a)anthracene (BaA), and benzo(a) pyrene (BaP). Hsu et al. [58] stated that graphene oxide aerogel could adsorb 0.310 μg g^{-1} BaP in 1h. Ref. [59] reported that petroleum coke-based activated carbon could adsorb 46 μg g^{-1} PHE. Although several studies have been performed on different PAHs removal techniques using different adsorbents, none performed a study on BghiP and IP removal techniques using NWAC. Hence, only one previous study was found on targeted pollutants of this study, but the BghiP and IP adsorption capacity of NWAC is remarkable compared to wood waste-derived biochar ref. [44].

4. Conclusion

In this study, NWAC was synthesized from the waste newspaper through pyrolysis at 800 °C for 3h with acid activation to remove carcinogenic pollutants, namely BghiP and IP.. Batch experiments were conducted to determine the optimum dosage, concentration, pH, and time. NWAC showed around 92% removal efficiency for both pollutants at optimum conditions. The adsorption behavior was best fitted for pseudo-second-order kinetics and Langmuir isotherm models. Regeneration studies confirmed its repeatable cycles of reusability. In real samples, the removal efficiency was estimated at 87.041% (BghiP) and 85.632% (IP), respectively. Hence, the developed NWAC adsorbent from recycled waste newspapers is a promising candidate for removing organic pollutants (BghiP and IP) from wastewater. This study will pave the way for future PAHs removal techniques by implying waste newspaper-driven activated carbon. NWAC-based activated carbon would be a promising adsorbent for developing technologies for removing trace metals, pesticides, antibiotics, dioxins, etc. This study has a limitation in terms of evaluating the environmental impacts as well as associated

potential risks using NWAC. Despite this limitation, this study is expected to support related research.

Author contribution statement

Aynun Nahar: Conceived and designed the experiments; Performed the experiments; Wrote the paper.
Md. Ahedul Akbor, Nushrat Jahan Chowdhury: Analyzed and interpreted the data; Wrote the paper.
Nigar Sultana Pinky: Performed the experiments; Wrote the paper.
Shamim Ahmed, Md. Abdul Gafur: Contributed reagents, materials, analysis tools or data.
Umme Sarmeen Akhtar, Md. Saiful Quddus, Fariha Chowdhury: Contributed reagents, materials, analysis tools or data; Analyzed and interpreted the data.

Data availability statement

Data included in article/supplementary material/referenced in article.

Funding

This work was carried out under the Research and Development (R & D) project entitled "Preparation of aerogel from waste paper for removing organic pollutants from wastewater" approved for the financial year of 2021–2023 by the authority of Bangladesh Council of Scientific and Industrial Research (BCSIR), Dhaka, Bangladesh.

Declaration of competing interest

The authors declare that they have no known competing financial interests or personal relationships that could have appeared to influence the work reported in this paper.

Appendix A. Supplementary data

Supplementary data to this article can be found online at https://doi.org/10.1016/j.heliyon.2023.e17793.

References

[1] G.G. Lauenstein, K.L. Kimbrough, Chemical contamination of the Hudson-Raritan Estuary as a result of the attack on the World Trade Center: analysis of polycyclic aromatic hydrocarbons and polychlorinated biphenyls in mussels and sediment, Mar. Pollut. Bull. 54 (2007) 284–294, https://doi.org/10.1016/j.marpolbul.2006.10.006.
[2] H. Xu, Q. Wang, X. Wang, W. Feng, F. Zhu, Diffusion of polycyclic aromatic hydrocarbons between water and sediment and their ecological risks in Wuhu city, Yangtze River Delta urban agglomerations, China, Appl, Geochemistry 119 (2020), 104627, https://doi.org/10.1016/j.apgeochem.2020.104627.
[3] M. Munir, M. Saeed, M. Ahmad, A. Waseem, M. Alsaady, S. Asif, A. Ahmed, M. Shariq Khan, A. Bokhari, M. Mubashir, L. Fatt Chuah, P. Loke Show, Cleaner production of biodiesel from novel non-edible seed oil (Carthamus lanatus L.) via highly reactive and recyclable green nano CoWO3@rGO composite in context of green energy adaptation, Fuel 332 (2023), 126265, https://doi.org/10.1016/j.fuel.2022.126265.
[4] L.F. Chuah, A. Bokhari, S. Asif, J.J. Klemeš, D.J. Dailin, H. El Enshasy, A.H.M. Yusof, A review of performance and emission characteristic of engine diesel fuelled by biodiesel, Chem. Eng. Trans. 94 (2022) 1099–1104, https://doi.org/10.3303/CET2294183.
[5] L.F. Chuah, A.R.A. Aziz, S. Yusup, J.J. Klemes, A. Bokhari, Waste cooking oil biodiesel via hydrodynamic cavitation on a diesel engine performance and greenhouse gas footprint reduction, Chem. Eng. Trans. 50 (2016) 301–306.
[6] M. Sadia, A. Mahmood, M. Ibrahim, M.K. Irshad, A.H.A. Quddusi, A. Bokhari, M. Mubashir, L.F. Chuah, P.L. Show, Microplastics pollution from wastewater treatment plants: a critical review on challenges, detection, sustainable removal techniques and circular economy, Environ. Technol. Innov. (2022), 102946.
[7] L.F. Chuah, K. Mokhtar, S.M.M. Ruslan, A.A. Bakar, M.A. Abdullah, N.H. Osman, A. Bokhari, M. Mubashir, P.L. Show, Implementation of the energy efficiency existing ship index and carbon intensity indicator on domestic ship for marine environmental protection, Environ. Res. 222 (2023), 115348.
[8] A.O. Adeniji, O.O. Okoh, A.I. Okoh, Distribution pattern and health risk assessment of polycyclic aromatic hydrocarbons in the water and sediment of Algoa Bay, South Africa, Environ. Geochem. Health 41 (2019) 1303–1320, https://doi.org/10.1007/s10653-018-0213-x.
[9] O. Duke, Source determination of polynuclear aromatic hydrocarbons in water and sediment of a creek in the Niger Delta region, Afr. J. Biotechnol. 7 (2008) 282–285, https://doi.org/10.5897/AJB07.098.
[10] K.W. Cheah, S. Yusup, L.F. Chuah, A. Bokhari, Physio-chemical studies of locally sourced non-edible oil: prospective feedstock for renewable diesel production in Malaysia, Procedia Eng. 148 (2016) 451–458.
[11] L.F. Chuah, J.J. Klemeš, A. Bokhari, S. Asif, Y.W. Cheng, C.C. Chong, P.L. Show, A review of intensification technologies for biodiesel production, Biofuels Biorefining (2022) 87–116.
[12] H. Services, Toxicological Profile for Polycyclic Aromatic Hydrocarbons (PAHS), ATSDR's Toxicol. Profiles, 2002, https://doi.org/10.1201/9781420061888_ch127.
[13] T.H. Pham, S.H. Jung, Y.J. Kim, T.Y. Kim, Adsorptive removal and recovery of organic pollutants from wastewater using waste paper-derived carbon-based aerogel, Chemosphere 268 (2021), 129319, https://doi.org/10.1016/j.chemosphere.2020.129319.
[14] L.F. Chuah, K.W. Chew, A. Bokhari, M. Mubashir, P.L. Show, Biodegradation of crude oil in seawater by using a consortium of symbiotic bacteria, Environ. Res. 213 (2022), 113721.
[15] E. Neyens, J. Baeyens, A review of classic Fenton's peroxidation as an advanced oxidation technique, J. Hazard Mater. 98 (2003) 33–50, https://doi.org/10.1016/S0304-3894(02)00282-0.
[16] T. Vescovi, H.M. Coleman, R. Amal, The effect of pH on UV-based advanced oxidation technologies - 1,4-Dioxane degradation, J. Hazard Mater. 182 (2010) 75–79, https://doi.org/10.1016/j.jhazmat.2010.06.001.

[17] C. Allègre, P. Moulin, M. Maisseu, F. Charbit, Treatment and reuse of reactive dyeing effluents, J. Membr. Sci. 269 (2006) 15–34, https://doi.org/10.1016/j.memsci.2005.06.014.

[18] C.M. Domínguez, A. Quintanilla, J.A. Casas, J.J. Rodriguez, Kinetics of wet peroxide oxidation of phenol with a gold/activated carbon catalyst, Chem. Eng. J. 253 (2014) 486–492, https://doi.org/10.1016/j.cej.2014.05.063.

[19] M. Ahmaruzzaman, Adsorption of phenolic compounds on low-cost adsorbents: a review, Adv. Colloid Interface Sci. 143 (2008) 48–67.

[20] N.B. Singh, G. Nagpal, S. Agrawal, Water purification by using adsorbents: a review, Environ. Technol. Innov. 11 (2018) 187–240.

[21] T. Zhang, D. Yuan, Q. Guo, F. Qiu, D. Yang, Z. Ou, Preparation of a renewable biomass carbon aerogel reinforced with sisal for oil spillage clean-up: inspired by green leaves to green Tofu, Food Bioprod. Process. 114 (2019) 154–162.

[22] Z. Jing, J. Ding, T. Zhang, D. Yang, F. Qiu, Q. Chen, J. Xu, Flexible, versatility and superhydrophobic biomass carbon aerogels derived from corn bracts for efficient oil/water separation, Food Bioprod. Process. 115 (2019) 134–142.

[23] P. Song, J. Cui, J. Di, D. Liu, M. Xu, B. Tang, Q. Zeng, J. Xiong, C. Wang, Q. He, Carbon microtube aerogel derived from kapok fiber: an efficient and recyclable sorbent for oils and organic solvents, ACS Nano 14 (2019) 595–602.

[24] A.S.M. Riyad, Scenario of paper waste recycling and reuse practices in Khulna city of Bangladesh, Int. J. Sci. Eng. Res. 5 (2014) 705–711.

[25] M. Beckline, S. Yujun, Z. Eric, M.S. Kato, Paper consumption and environmental impact in an emerging economy, J. Energy, Environ. Chem. Eng. 1 (2016) 13–18.

[26] G. Aylaz, M. Okan, M. Duman, H.M. Aydin, Study on cost-efficient carbon aerogel to remove antibiotics from water resources, ACS Omega 5 (2020) 16635–16644.

[27] K. Li, M. Zhou, L. Liang, L. Jiang, W. Wang, Ultrahigh-surface-area activated carbon aerogels derived from glucose for high-performance organic pollutants adsorption, J. Colloid Interface Sci. 546 (2019) 333–343.

[28] Y. Wang, W. Tian, C. Wu, J. Bai, Y. Zhao, Synthesis of coal cinder balls and its application for CODCr and ammonia nitrogen removal from aqueous solution, Desalination Water Treat. 57 (2016) 21781–21793.

[29] K. Qiao, W. Tian, J. Bai, J. Dong, J. Zhao, X. Gong, S. Liu, Preparation of biochar from Enteromorpha prolifera and its use for the removal of polycyclic aromatic hydrocarbons (PAHs) from aqueous solution, Ecotoxicol. Environ. Saf. 149 (2018) 80–87.

[30] L. Muniandy, F. Adam, A.R. Mohamed, E.P. Ng, The synthesis and characterization of high purity mixed microporous/mesoporous activated carbon from rice husk using chemical activation with NaOH and KOH, Microporous Mesoporous Mater. 197 (2014) 316–323, https://doi.org/10.1016/j.micromeso.2014.06.020.

[31] D. Lv, Y. Li, L. Wang, Carbon aerogels derived from sodium lignin sulfonate embedded in carrageenan skeleton for methylene-blue removal, Int. J. Biol. Macromol. 148 (2020) 979–987.

[32] M. Hartman, O. Trnka, M. Pohořelý, Minimum and terminal velocities in fluidization of particulate ceramsite at ambient and elevated temperature, Ind. Eng. Chem. Res. 46 (2007) 7260–7266.

[33] B. Özkaya, Adsorption and desorption of phenol on activated carbon and a comparison of isotherm models, J. Hazard Mater. 129 (2006) 158–163.

[34] S. Varjani, G. Kumar, E.R. Rene, Developments in biochar application for pesticide remediation: current knowledge and future research directions, J. Environ. Manag. 232 (2019) 505–513.

[35] Y. Cao, B. Yang, Z. Song, H. Wang, F. He, X. Han, Wheat straw biochar amendments on the removal of polycyclic aromatic hydrocarbons (PAHs) in contaminated soil, Ecotoxicol. Environ. Saf. 130 (2016) 248–255.

[36] D. Tan, J. Zhao, C. Gao, H. Wang, G. Chen, D. Shi, Carbon nanoparticle hybrid aerogels: 3D double-interconnected network porous microstructure, thermoelectric, and solvent-removal functions, ACS Appl. Mater. Interfaces 9 (2017) 21820–21828.

[37] Q. Luo, H. Zheng, Y. Hu, H. Zhuo, Z. Chen, X. Peng, L. Zhong, Carbon nanotube/chitosan-based elastic carbon aerogel for pressure sensing, Ind. Eng. Chem. Res. 58 (2019) 17768–17775.

[38] P. Devi, A.K. Saroha, Effect of pyrolysis temperature on polycyclic aromatic hydrocarbons toxicity and sorption behaviour of biochars prepared by pyrolysis of paper mill effluent treatment plant sludge, Bioresour. Technol. 192 (2015) 312–320.

[39] Y. Li, Q. Du, X. Wang, P. Zhang, D. Wang, Z. Wang, Y. Xia, Removal of lead from aqueous solution by activated carbon prepared from Enteromorpha prolifera by zinc chloride activation, J. Hazard Mater. 183 (2010) 583–589.

[40] V.K. Garg, R. Gupta, A.B. Yadav, R. Kumar, Dye removal from aqueous solution by adsorption on treated sawdust, Bioresour. Technol. 89 (2003) 121–124.

[41] H. Gupta, R. Kumar, Removal of PAH anthracene from aqueous media using banana peel activated carbon, Int. J. Sci. Res. Environ. Sci. 4 (2016) 109–114.

[42] S.-Y. Oh, Y.-D. Seo, Factors affecting the sorption of halogenated phenols onto polymer/biomass-derived biochar: effects of pH, hydrophobicity, and deprotonation, J. Environ. Manag. 232 (2019) 145–152.

[43] Y.R. Corrales Ureña, L. Wittig, M. Vieira Nascimento, J.L. Faccioni, P.N. Lisboa Filho, K. Rischka, Influences of the pH on the adsorption properties of an antimicrobial peptide on titanium surfaces, Appl. Adhes. Sci. 3 (2015) 1–17.

[44] A.M. Carvajal-Bernal, F. Gómez, L. Giraldo, J.C. Moreno-Piraján, Adsorption of phenol and 2, 4-dinitrophenol on activated carbons with surface modifications, Microporous Mesoporous Mater. 209 (2015) 150–156.

[45] B. Adane, K. Siraj, N. Meka, Kinetic, equilibrium and thermodynamic study of 2-chlorophenol adsorption onto Ricinus communis pericarp activated carbon from aqueous solutions, Green Chem. Lett. Rev. 8 (2015) 1–12.

[46] I. Langmuir, The adsorption of gases on plane surfaces of glass, mica and platinum, J. Am. Chem. Soc. 40 (1918) 1361–1403.

[47] J. Cao, Y. Ma, Direct preparation of activated carbon fiber aerogel via pyrolysis of cotton under CO2 atmosphere and its adsorption of methylene blue, Energy Sources, Part A Recover, Util. Environ. Eff. 42 (2020) 1108–1117, https://doi.org/10.1080/15567036.2019.1602221.

[48] S. Rangabhashiyam, N. Anu, M.S.G. Nandagopal, N. Selvaraju, Relevance of isotherm models in biosorption of pollutants by agricultural byproducts, J. Environ. Chem. Eng. 2 (2014) 398–414.

[49] X. Zhou, L. Shi, T.B. Moghaddam, M. Chen, S. Wu, X. Yuan, Adsorption mechanism of polycyclic aromatic hydrocarbons using wood waste-derived biochar, J. Hazard Mater. 425 (2022), 128003.

[50] J.H.F. De Jesus, G. da C. Cunha, E.M.C. Cardoso, A.S. Mangrich, L.P.C. Romão, Evaluation of waste biomasses and their biochars for removal of polycyclic aromatic hydrocarbons, J. Environ. Manag. 200 (2017) 186–195.

[51] S. Gul, Z. Ahmad, M. Asma, M. Ahmad, K. Rehan, M. Munir, A.A. Bazmi, H.M. Ali, Y. Mazroua, M.A. Salem, Effective adsorption of cadmium and lead using SO3H-functionalized Zr-MOFs in aqueous medium, Chemosphere 307 (2022), 135633.

[52] T.B. Boving, W. Zhang, Removal of aqueous-phase polynuclear aromatic hydrocarbons using aspen wood fibers, Chemosphere 54 (2004) 831–839, https://doi.org/10.1016/j.chemosphere.2003.07.007.

[53] J.A. Mattson, H.B. Mark Jr., M.D. Malbin, W.J. Weber Jr., J.C. Crittenden, Surface chemistry of active carbon: specific adsorption of phenols, J. Colloid Interface Sci. 31 (1969) 116–130.

[54] Z.Z. Li, Q. Sun, H. Zhu, Z.Y. Liu, Study on sorption behaviors and influence factors of polycyclic aromatic hydrocarbon fluoranthene on surface sediment in the Jialing River, Environ. Ecol. Three Gorges. 34 (2012) 31–36.

[55] X. Wang, Z. Guo, Z. Hu, H.H. Ngo, S. Liang, J. Zhang, Adsorption of phenanthrene from aqueous solutions by biochar derived from an ammoniation-hydrothermal method, Sci. Total Environ. 733 (2020), 139267, https://doi.org/10.1016/j.scitotenv.2020.139267.

[56] E. Daneshvar, A. Vazirzadeh, A. Niazi, M. Kousha, M. Naushad, A. Bhatnagar, Desorption of methylene blue dye from brown macroalga: effects of operating parameters, isotherm study and kinetic modeling, J. Clean. Prod. 152 (2017) 443–453.

[57] Y. Dai, J. Niu, L. Yin, J. Xu, J. Xu, Laccase-carrying electrospun fibrous membrane for the removal of polycyclic aromatic hydrocarbons from contaminated water, Sep. Purif. Technol. 104 (2013) 1–8.
[58] H. Hsu, C. Kuo, J. Jehng, C. Wei, C. Wen, J. Chen, L. Chen, Application of graphene oxide aerogel to the adsorption of polycyclic aromatic hydrocarbons emitted from the diesel vehicular exhaust, J. Environ. Chem. Eng. 7 (2019), 103414, https://doi.org/10.1016/j.jece.2019.103414.
[59] M. Yuan, S. Tong, S. Zhao, C.Q. Jia, Adsorption of polycyclic aromatic hydrocarbons from water using petroleum coke-derived porous carbon, J. Hazard Mater. 181 (2010) 1115–1120.